Wind Profile Measurement Using Lifting Sensors

ROBERT F. STENGEL*
Princeton University, Princeton, N. J.

A vertical profile of wind velocity for use in rocket prelaunch operations should be measured rapidly in order to minimize the space-time displacement between the measured profile and the ascent trajectory. A lifting wind sensor, a missile-like body with a large cruciform or annular wing, can measure the wind profile below 100,000 ft in 10 to 15 min. Using the linearized equations of motion to determine the wind response transfer function, a sample configuration is shown to have a maximum resolution more than an order of magnitude better than that of a drag wind sensor, e.g., balloon, chaff, or parachute, with the same fall velocity. Although the maximum resolution is set by the ratio $2m_e/C_{L\alpha}S\rho$, the amplitude and phase fidelity largely depend on the moment stability derivatives. The response to arbitrary profiles, computed with a three-degree-of-freedom trajectory program, supports the linear analysis. By employing an iterative technique, the accuracy of the wind-profile estimate can be increased by at least an order of magnitude. Preliminary flight test data are briefly discussed.

Nomenclature

A, B, C, D = transfer function numerator and denominator coefficients
AR = amplitude ratio, decibels or linear scale
c = mean aerodynamic chord, ft
C_D = drag or axial force coefficient
C_L = lift or normal force coefficient
C_m = pitch moment coefficient
D_u = $C_D\rho US/m$ (ignoring compressibility)
D_α = $2C_LC_{L\alpha}QS/\pi eAm$
g = gravitational acceleration, 32.2 ft/sec^2
I_y = longitudinal moment of inertia, slug-ft^2
L = response length, ft
L_u = $C_L\rho US/m$ (ignoring compressibility and aeroelasticity)
L_α = $C_{L\alpha}QS/m$
$L_{\dot\alpha}$ = $C_{L\dot\alpha}\rho USc/m$
$L_{\dot\theta}$ = $C_{L_q}\rho USc/m$
m = mass, slugs
m' = apparent mass, slugs
m_e = $m + m'$, slugs
M_u = $C_L(SM)\rho US/I_y$
M_α = $C_{L\alpha}(SM)QS/I_y$
$M_{\dot\alpha}$ = $C_{m\dot\alpha}\rho USc^2/4I_y$
$M_{\dot\theta}$ = $C_{mq}\rho USc^2/4I_y$
N = transfer function numerator
q = pitch rate, deg (or rad)/sec
Q = dynamic pressure, psf
s = Laplace operator = $\mathcal{L}[(d/dt)()]$
S = reference area, ft^2
SM = static margin = distance between center of gravity and aerodynamic center, ft
t = time, sec
u, w = body-fixed axial and normal velocities, fps
U = total velocity, fps
x, z = earth-fixed horizontal and vertical displacement, ft
$\dot X$ = Laplace transform of $\dot x(t) = \mathcal{L}[\dot x(t)]$
$z_{1,2}$ = transfer function zeroes, sec^{-1}
α = angle of attack, deg or rad
β = inverse of air density scale height, ft^{-1}
Δ = characteristic equation
ϵ = average error, fps
ζ = damping ratio
θ = pitch attitude angle (to horizontal), deg or rad
λ = wavelength, ft; real root of characteristic equation, sec^{-1}
ρ = air density, slug/ft^3
τ = time const, sec
ϕ = phase angle, deg or rad
ω = circular frequency, rad/sec
ω_n = natural frequency, rad/sec

Special notation

$(\dot{\ })$ = differentiation with respect to time
$(\ )_x$ = differentiation with respect to x
$(\ )^*$ = effective input coefficient
$\Delta(\ )$ = perturbation quantity

Subscripts

a = with respect to the air
0 = initial value
PS = path stability mode
SP = short period mode
T = aerodynamically tuned
v = velocity mode
w = normal velocity numerator
W = wind input
$\dot x$ = horizontal velocity numerator
θ = pitch attitude numerator

Presented as Preprint 65-15 at the AIAA 2nd Aerospace Sciences Meeting, New York, January 25–27, 1965; submitted January 6, 1965; revision received August 5, 1965.

* Graduate Student, Department of Aerospace and Mechanical Sciences. Member AIAA.

Introduction

AT low altitudes, local geography causes significant horizontal, as well as vertical, variations in the wind velocity. Above this region, horizontal variations are smaller, but the vertical gradient still is important; consequently, a vertical profile of the wind velocity adequately describes the wind field within a limited geographic region. Since the wind sensor may take a period of time to traverse the atmosphere, moving horizontally in the process, the measured profile generally is neither vertical nor instantaneous. Wind data collected to meet an operational requirement, e.g., for a rocket launch, must be obtained near the rocket's ascent path and close to launch time. Trajectory deviations may be produced by winds at altitudes up to 100,000 ft, with those below 60,000 ft more important because of high atmospheric density, wind velocity, and wind shear.[1–3] With respect to structural loads, the region between 25,000 and 40,000 ft is most important, for here maximum jetstream velocity, maximum dynamic pressure, and transonic Mach numbers are coincident. High resolution in wind data is particularly important in this region.

A final requirement on prelaunch wind profile measurement is that it be done as quickly as possible. If random failure in equipment occurs, operations may be held up while measurements are repeated. Since men, precision tracking equipment, and computing equipment are involved, a long measurement time is costly. A short time is also desirable when multiple measurements are needed to support successive launch operations.

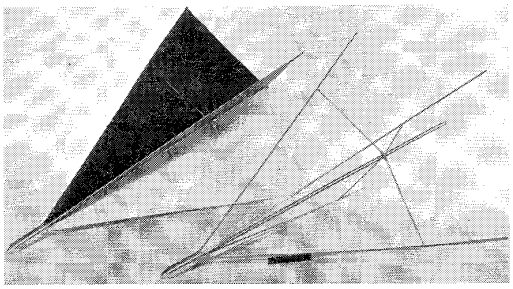

Fig. 1 A typical lifting sensor configuration: cruciform triangular wing, Mylar and aluminum structure.

Existing measurement techniques[4–12] include the following: 1) a vertically dispensed trail of smoke can be photographed at regular intervals[4–6]; this method provides precision data, but it can be used only under near-perfect visibility conditions in the daylight hours; 2) a similar technique, employing a vertical trail of radar-refective chaff with Doppler tracking, has also been investigated analytically[7]; 3) the Shearsonde[8] now in development is an instrumented, missile-like probe that measures the wind shear profile, through wind-induced normal accelerations telemetered to a ground station; 4) angle-of-attack measurements made by an ascending rocket vehicle can be combined with trajectory and attitude data to obtain the wind profile[7]; and 5) a drag wind sensor, such as balloon, chaff cloud, or parachute, drifts with the wind as it rises or falls through the atmosphere; since lift forces generally arise in a random fashion, they are not used to advantage; rather, they introduce errors in the wind measurement. The wind profile is obtained by radio tracking methods, such as rawinsonde and pulse radar systems. Neither of the operational methods, 1 and 5, is entirely suitable for the prelaunch measurement. Although the smoke trail measurement is virtually instantaneous, reduction of the data is a time-consuming process, and the visibility requirement precludes all-weather use. The drag sensor cannot provide both high resolution and fast measurement; in addition to being undesirable in its own right, a long measurement time allows the sensor to drift far from its release point by the end of the measurement period.

This paper presents an analysis of the wind-measuring capability of a lifting sensor, which is tracked by radio methods and which falls rapidly from its release altitude, deviating from a vertical path as a result of wind-induced normal forces. The wind response of the lifting sensor is determined using both the linearized equations of motion and a three-degree-of-freedom digital-computer trajectory program. Step response, frequency response, and response to arbitrary wind profiles are presented and compared with results of a limited flight test program. An iterative method of reducing dynamic errors is investigated.

Lifting Wind Sensor

The sensor is a statically stable missile-like configuration (Fig. 1) possessing 120° or higher-order rotational symmetry about its longitudinal axis. With zero trim lift coefficient and in the absence of wind, the sensor falls vertically, with its longitudinal axis aligned to the vertical because of static stability. The wind response is a result of the normal force provided by the wind-induced angle of attack. A possible operational sequence is shown in Fig. 2. The sensor is folded and stored within the "dart" of a booster-dart meteorological rocket. The rocket carries the sensor to 100,000 ft in 1 min, at which time a pyrotechnic or mechanical fuze ejects it. The sensor takes its shape through spring-loading, prestressing, or self-inflation and begins its fall.

Throughout this analysis, the following assumptions are made: 1) the lifting sensor is an axisymmetric, nonspinning, rigid body with zero trim lift coefficient; 2) wind sensitivity can be described by the two-dimensional case, with three degrees of freedom (vertical and horizontal translation and pitch rotation); 3) aerodynamic coefficients C_D, C_L, C_m and their derivatives are independent of Mach number M, Reynolds number Re, and angle of attack α; 4) rotation and sphericity of the earth are unimportant to the sensor's dynamics; and 5) time variation of the profile produces no forces or moments on the sensor.

Assumption 1 limits the scope of this investigation. Asymmetry, roll coupling, gyroscopic stability, and aeroelasticity could produce significant effects and should be the subject of further study. As a result of symmetry and zero roll, small-amplitude lateral and longitudinal oscillations are essentially independent. Since three-degree-of-freedom computer studies indicate that the most severe wind profiles do not perturb α and pitch attitude θ by more than a few degrees, assumption 2 can be made. For a configuration with 120° or higher-order rotational symmetry, the wind input and sensor output occur within the same plane, and small-amplitude response is independent of roll orientation.[13] For typical configurations, M will be less than 0.8 and $Re > 10^5$ below 100,000 ft, and α remains small (variations in C_D and nonlinearities in $C_{L\alpha}$ and the damping derivatives are negligible); hence assumption 3 is reasonable. With the exception of $\dot{\alpha}$ derivatives, aerodynamic derivatives are based on steady flow. For this application, coriolis and centrifugal accelerations due to a round, rotating earth and the variation in gravity with altitude are negligible, allowing assumption 4. Assumption 5 requires wind velocity and wind shear to be frozen for a duration of less than 0.1 sec as the sensor passes a fixed point.

The cruciform triangular wing sensor shown in Fig. 1 was chosen for initial studies because it could be folded and stored within a meteorological dart, and because such a configuration has been built and flight-tested at the NASA Wallops Station. It is 4.5 ft long and has a wing span of 3.4 ft and a wing area of 6.8 ft^2. It is constructed of $\frac{1}{2}$-mil alumin-

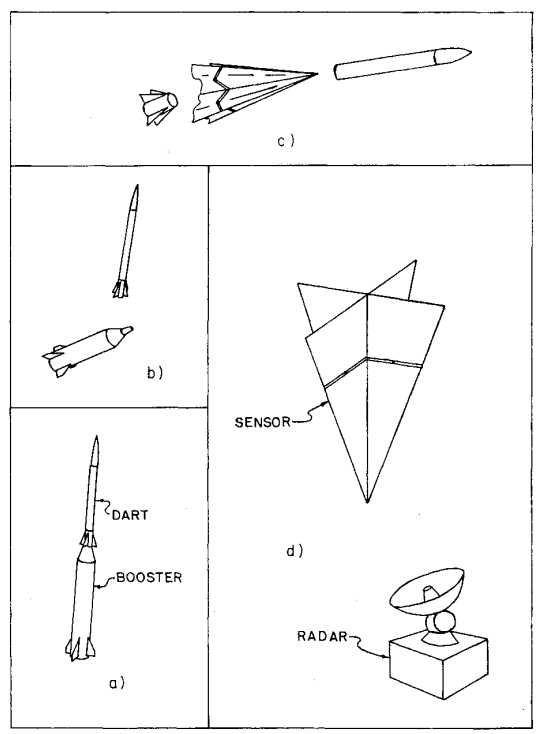

Fig. 2 A possible operational sequence for the lifting sensor: a) launch of booster-dart meteorological rocket; b) separation of dart; c) ejection of sensor above 100,000-ft altitude; and d) descent of sensor.

ized Mylar on a frame of $\frac{1}{4}$-in. aluminum rod and weighs 3.2 lb.

With the exception of C_D, which was determined from flight-test data, the nondimensional coefficients were calculated by slender wing theory and Bryson's method.[14] The dimensional stability derivatives, with units of acceleration per unit change in the perturbation variable, are computed using these coefficients. For example,

$$L_\alpha = (1/m)\partial L/\partial\alpha = C_{L\alpha}\rho U^2 S/2m \tag{1}$$

and

$$M_\alpha = (1/I_y)\partial M/\partial\alpha = C_{L\alpha}(SM)\rho U^2 S/2I_y \tag{2}$$

With a piecewise-exponential fit to the U. S. Standard Atmosphere, 1962, both ρ and U are determined at any altitude. Assuming that vertical acceleration is nonzero but constant, the equilibrium fall velocity is

$$U = \dot{z} = [2mg/(C_D S\rho - m\beta)]^{1/2} \tag{3}$$

where β is the inverse of the "scale height" of the exponential density approximation.

Dynamic Response

Linearized Equations of Motion

The digital trajectory simulation discussed later indicates that α and θ responses to typical wind inputs are small. With the assumptions noted previously, the wind response of the lifting sensor can be described by the linearized aircraft longitudinal equations of motion.[13–17] Aerodynamic forces and moments are expanded as Taylor series in the perturbation variables Δu, Δw, $\Delta\theta$, and their time rates of change, retaining only first-order terms. The coefficients of these series, the dimensional stability derivatives, vary only slowly with time (or altitude) and may be considered quasi-constant. The assumption of constant coefficients also requires that wind input wavelengths be large compared to the sensor's length, in order that frequency-dependent, unsteady flow effects do not become significant.

The kinematic relationship between the body-fixed inertial velocities u and w and the earth-fixed inertial velocities $\dot{x}$ and $\dot{z}$ is given by the equations

$$\dot{x} = u\cos\theta + w\sin\theta \qquad \dot{z} = -u\sin\theta + w\cos\theta \tag{4}$$

where θ is referenced to the horizontal (hence $\theta_0 = -90°$), and u, w, θ, $\dot{x}$, and $\dot{z}$ are defined as sums of initial and perturbation variables (e.g., $u = u_0 + \Delta u$), Considering only first-order terms and applying small-angle assumptions about θ_0,

$$\dot{x} = u_0\Delta\theta - (w_0 + \Delta w) \qquad \dot{z} = (u_0 + \Delta u) + w_0\Delta\theta \tag{5}$$

and

$$\Delta\dot{x} = u_0\Delta\theta - \Delta w \qquad \Delta\dot{z} = \Delta u + w_0\Delta\theta \tag{6}$$

The air relative velocities are related to the inertial and wind velocities by the equations

$$\Delta u_a = \Delta u + \Delta u_W \qquad \Delta w_a = \Delta w + \Delta w_W \tag{7}$$

where the subscript W denotes the body-fixed components of the wind velocity. Since the wind is assumed to be purely horizontal, these components are

$$\Delta u_W = -\Delta\dot{x}_W\cos\theta \simeq 0 \qquad \Delta w_W = -\Delta\dot{x}_W\sin\theta \simeq \Delta\dot{x}_W \tag{8}$$

Recognizing that the inertial terms will be multiplied by inertial variables and the stability derivatives by aerodynamic variables, the equations of motion can be written in terms of Δu, Δw, and $\Delta\theta$, with Δu_W and Δw_W appearing as forcing functions. With zero initial conditions, the linearized equations, expressed in Laplace notation, are as follows:

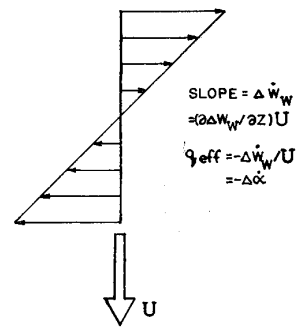

Fig. 3 The velocity distribution on the sensor due to wind shear is the same as that due to a rotational rate.

Axial Force

$$(s + D_u)\Delta u + D_\alpha(\Delta w/U) = -D_\alpha(\Delta w_W/U) - D_u\Delta u_W \tag{9}$$

Normal Force

$$L_u\Delta u + \left[\left(1 + \frac{L_{\dot\alpha}}{U}\right)s + \frac{L_\alpha}{U}\right]\Delta w + U\left[\left(\frac{L_{\dot\theta}}{U} - 1\right)s - \frac{g}{U}\right]\Delta\theta = -\left(\frac{L_{\dot\alpha}{}^*s + L_\alpha}{U}\right)\Delta w_W - L_u\Delta u_u \tag{10}$$

Pitch Moment

$$-M_u\Delta u - (M_{\dot\alpha}s + M_\alpha)(\Delta w/U) + s(s - M_{\dot\theta})\Delta\theta = (M_{\dot\alpha}{}^*s + M_\alpha)(\Delta w_W/U) + M_u\Delta u_W \tag{11}$$

To emphasize the correspondence between α and w [$\Delta\alpha = \tan^{-1}(\Delta w/u) \simeq \Delta w/U$], the subscript α has been retained.

Among the forcing functions on the right side of the equations, there are terms containing not only the magnitude of the wind input but also its time rate of change. It should be clear that the aerodynamic forces induced by the motion of the sensor will be induced by the apparent motion due to a time-varying input. It is less apparent that $\dot{w}_W$ produces an effective pitch rate q_{eff} in addition to $\dot{\alpha}$; however, this can be seen in Fig. 3. A constant $\dot{w}_W$ produces a velocity distribution along the length of the sensor which is identical to the distribution caused by a pitch rate of opposite sign.[13] It is necessary, therefore, to account for the forcing of the system by both $\dot{\alpha}$ and q_{eff} using the derivatives marked by asterisks, $L_{\dot\alpha}{}^* = L_{\dot\alpha} - L_{\dot\theta}$, and $M_{\dot\alpha}{}^* = M_{\dot\alpha} - M_{\dot\theta}$.

The characteristic equation, obtained by taking the determinant of the coefficient matrix of Eqs. (9–11), is of the form

$$\begin{aligned}\Delta &= A_4s^4 + A_3s^3 + A_2s^2 + A_1s + A_0 \\ &= A_4(s - \lambda_v)(s - \lambda_{PS})(s^2 + 2\zeta_{SP}\omega_{nSP}s + \omega_{nSP}{}^2)\end{aligned} \tag{12}$$

In level flight, the airplane characteristic equation factors into two complex pairs representing the phugoid and short-period modes; however, in near-vertical flight, the phugoid pair degenerates into two real roots.[16] The first, which might be called the velocity mode, is typically convergent for a nonthrusting, falling aircraft, since $\lambda_v \simeq -D_u$, and D_u is usually positive. The path stability mode is always divergent for rising aircraft and convergent for falling aircraft. (For buoyant objects, the opposite is true.) The root is approximately $\lambda_{PS} = 1/\tau_{PS} \simeq g/\dot{z}$. This is the dynamic mode through which the drag sensor responds to the wind.

Since the sample configuration is assumed to have zero trim lift coefficient, D_α, which is proportional to C_L, is zero. With no compressibility or aeroelastic effects, $L_u = M_u = 0$. Therefore, Eq. (9) is uncoupled from (10) and (11), and the

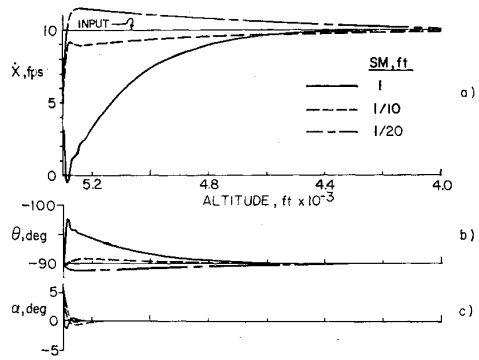

Fig. 4 Step response of the lifting sensor at an altitude of 5300 ft for three values of static margin (SM): a) horizontal velocity response; b) pitch attitude response; and c) angle-of-attack response.

linear wind sensitivity can be determined from the latter set of equations, which is reduced to the following:

Normal Force

$$\left[\left(1 + \frac{L_{\dot\alpha}}{U}\right) s + \frac{L_\alpha}{U}\right] \Delta w + U \left[\left(\frac{L_{\dot\theta}}{U} - 1\right) s - \frac{g}{U}\right]\Delta\theta = -\left(\frac{L_{\dot\alpha}{}^* s + L_\alpha}{U}\right) \Delta w_W \quad (13)$$

Pitch Moment

$$-(M_{\dot\alpha} s + M_\alpha)(\Delta w/U) + s(s - M_{\dot\theta})\Delta\theta = (M_{\dot\alpha}{}^* s + M_\alpha)(\Delta w_W/U) \quad (14)$$

The characteristic equation is obtained as before, using the coefficients of Eqs. (13) and (15):

$$\Delta = A_3 s^3 + A_2 s^2 + A_1 s + A_0 \quad (15)$$

where

$$A_0 = -M_\alpha g/U$$

$$A_1 = -L_\alpha M_{\dot\theta}/U - M_{\dot\alpha} g/U - (1 - L_\theta/U)M_\alpha$$

$$A_2 = L_\alpha/U - (1 + L_{\dot\alpha}/U)M_{\dot\theta} - (1 - L_{\dot\theta}/U)M_{\dot\alpha}$$

$$A_3 = 1 + L_{\dot\alpha}/U$$

The characteristic equation takes the factored form:

$$\Delta = A_3(s - \lambda_{PS})(s^2 + 2\zeta_{SP}\omega_{nSP} s + \omega_{nSP}{}^2) \quad (16)$$

Wind Response Transfer Function

The wind response transfer function, which relates sensor horizontal velocity to wind velocity, is, from Eq. (6),

$$\Delta\dot X/\Delta\dot X_W = U\Delta\theta/\Delta\dot X_W - \Delta w/\Delta\dot X_W = (UN_\theta - N_W)/\Delta = N_{\dot x}/\Delta \quad (17)$$

where N_θ and N_W are the numerators of the pitch attitude and normal velocity transfer functions, and $u_0 = U$. The component transfer functions are found by Cramer's rule. The numerators are obtained by replacing the appropriate column of the coefficient matrix with the input coefficient column and finding the determinant:

$$N_\theta = (B_2 s^2 + B_1 s)(1/U) \quad (18)$$

where

$$B_1 = (1 + L_{\dot\theta}/U)M_\alpha - L_\alpha M_{\dot\theta}/U$$

$$B_2 = (1 + L_{\dot\theta}/U)M_{\dot\alpha} - (1 + L_{\dot\alpha}/U)M_{\dot\theta}$$

and

$$N_w = C_3 s^3 + C_2 s^2 + C_1 s + C_0 \quad (19)$$

where

$$C_0 = M_\alpha g/U$$

$$C_1 = (L_\alpha - g)M_{\dot\theta}/U + (1 - L_{\dot\theta}/U)M_\alpha + M_\alpha g/U$$

$$C_2 = -L_\alpha/U - (1 - L_{\dot\alpha}/U)M_\theta + (1 - L_{\dot\theta}/U)M_{\dot\alpha}$$

$$C_3 = (L_{\dot\theta} - L_{\dot\alpha})/U$$

Combining the two, the wind response numerator is

$$N_{\dot x} = -C_3 s^3 + (B_2 - C_2)s^2 + (B_1 - C_1)s - C_0 = D_3 s^3 + D_2 s^2 + D_1 s + D_0 \quad (20)$$

where

$$D_0 = -M_\alpha g/U$$

$$D_1 = 2L_{\dot\theta}M_\alpha/U - (2L_\alpha - g)M_{\dot\theta}/U - M_{\dot\alpha} g/U$$

$$D_2 = 2L_{\dot\theta}M_{\dot\alpha}/U - 2L_{\dot\alpha}M_{\dot\theta}/U + L_\alpha/U$$

$$D_3 = (L_{\dot\alpha} - L_{\dot\theta})/U$$

Equation (20) typically factors into three real roots, although it is possible to obtain a complex pair. Since Bryson's method[14] indicates that $L_{\dot\alpha} = L_{\dot\theta}$, the numerator is reduced to second order for the majority of cases considered here. The wind response transfer function is Eq. (20) divided by Eq. (15). With $L_{\dot\alpha} = L_\theta$ and $D_0 = A_0$, it generally takes the form

$$\frac{\Delta\dot X}{\Delta\dot X_W} = \frac{[(s/z_1) - 1][(s/z_2) - 1]}{[(s/\lambda_{PS}) - 1][(s^2/\omega_{nSP}{}^2) + 2(\zeta_{SP}/\omega_{nSP})s + 1]} \quad (21)$$

Step Response

Figures 4 and 5 show the wind sensor's response to a step input, calculated with the three-degree-of-freedom trajectory program. These results, which include the effects of changing altitude, dynamic pressure increment due to wind, and induced drag, could have been closely simulated by taking the inverse Laplace transform of $(A/s)(\Delta\dot X/\Delta\dot X_W)$, where A/s is the Laplace transform of a step input with amplitude

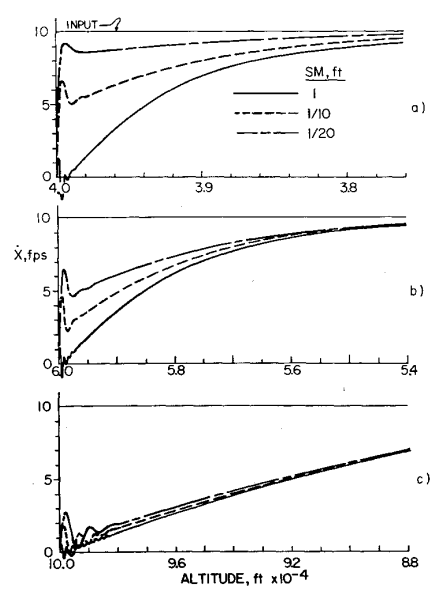

Fig. 5 Horizontal velocity response to step inputs at a) 40,000 ft, b) 60,000 ft, and c) 100,000 ft.

A. The corresponding time response would be of the form

$$\dot{x}(t) = A + K_{PS}e^{-\lambda_{PS}t} + K_{SP}e^{-\zeta_{SP}\omega_{nSP}t}\cos(\omega_{nSP}t + \phi_{SP}) \tag{22}$$

The response to 10-fps gusts beginning at 5300, 40,000, 60,000, and 100,000 ft were calculated for configurations with static margins (SM) of 1.0, 0.1, and 0.05 ft. It has been assumed that the change in SM affects only M_α and not the damping derivatives.

The wind response mechanism is shown in Fig. 4. Referring first to the 1.0-ft case, it can be seen that the wind input is similar to an initial condition on α. The high static stability produces a quick pitch response, as the sensor seeks $\alpha = 0$. In this case, the damping is not sufficient to prevent α overshoot. Before the overshoot occurs, the wing lift is accelerating the sensor with the wind, but during the overshoot the lift is reversed to the extent that $\dot{x}$ briefly changes sign. Although α soon goes to zero, θ is still several degrees from the vertical, and $\dot{x}$ is slowly approaching the wind velocity. The wind response mode is essentially the path stability mode, and the sensor's wings have had negligible effect on the wind measurement.

Reducing SM (or M_α) to 0.1 ft makes the pitch response more sluggish and prolongs the time to overshoot. The additional period of $\alpha > 0$ allows $\dot{x}$ to reach 92% of the wind velocity before adverse lift occurs. Since ω_{nSP} has been reduced but $\zeta_{SP}\omega_{nSP}$ has not, the damping ratio is increased, and the adverse lift has little effect. This configuration takes advantage of the sensor's wings, for the wind response is primarily due to the short-period mode. After the short-period response dies out, the slow climb to full response is left to the path stability mode. The path stability time constant is increased by the reduced static margin, and this configuration takes longer to reach full response than the first.

Further reduction of SM to 0.05 ft results in an overshoot in $\dot{x}$ response. This is accompanied by a pitch response of opposite sign. The static stability has been reduced to the point that it is weaker than the damping moments generated in passing through the step input. (In the previous two cases, the high shear produced by the step produces a barely perceptible pitch response of opposite sign; however, in both cases M_α is strong enough to cause the sensor to "weathercock" or nose into the wind after passing through the step.) As a result, the lifting acceleration continues in the wind direction past the point at which $\dot{x} = \dot{x}_W$. Since this configuration is statically stable, $\dot{x}$ eventually returns to $\dot{x}_W$ as θ returns to $-90°$. Although this case overresponds, it does not assume an equilibrium glide.

That it is possible for the sensor to overrespond, and that this condition corresponds to pitch response of opposite sign, indicates that there is a combination of aerodynamic coefficients which yields no pitch response to any wind input. This combination, called "aerodynamic tuning" by Larrabee,[8] is found by setting $N_\theta = 0$. Since there are s and s^2 terms, θ responds to both the wind magnitude and its time rate of change. The requirements for tuning are that

$$B_1 = 0 \quad \text{or} \quad (1 + L_{\dot{\theta}}/U)M_\alpha = L_\alpha M_{\dot{\theta}}/U \tag{23}$$

$$B_2 = 0 \quad \text{or} \quad (1 + L_{\dot{\theta}}/U)M_{\dot{\alpha}} = (1 + L_{\dot{\alpha}}/U)M_{\dot{\theta}} \tag{24}$$

With $L_{\dot{\theta}} = 0$, Eq. (23) is equivalent to Larrabee's tuning condition. Since $\Delta\theta = 0$ in the tuned condition, the rotational degree of freedom does not enter the wind response. The response is determined from the normal force equation alone, which reduces to

$$[(1 + L_{\dot{\alpha}}/U)s + L_\alpha/U]\Delta w = -(L_{\dot{\alpha}}{}^*s + L_\alpha)\Delta w_W/U \tag{25}$$

or

$$\Delta\dot{X}/\Delta\dot{X}_W = -\Delta w/\Delta w_W = (L_{\dot{\alpha}}{}^*s + L_\alpha)/[(U + L_{\dot{\alpha}})s + L_\alpha] \tag{26}$$

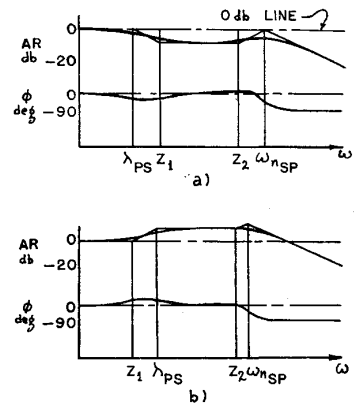

Fig. 6 Typical horizontal velocity frequency response curves illustrating amplitude ratio (AR) asymptotes and curves and phase angles (ϕ) for a) undertuned case, and b) overtuned case.

The root of this first-order equation is

$$\lambda_T = 1/\tau_T = L_\alpha/(U + L_{\dot{\alpha}}) = C_{L\alpha}S\rho\dot{z}/2m_e \tag{27}$$

and the tuned response length

$$L_T = \tau_T\dot{z} = 2m_e/C_{L\alpha}\rho S \tag{28}$$

is independent of U. It is interesting to note that, by replacing $L_{\dot{\alpha}}/U$ by m'/m and L_α/U by $C_DS\rho\dot{z}/2m$, and setting $L_{\dot{\theta}} = 0$, Eq. (25) becomes

$$(s + C_DS\rho\dot{z}/2m_e)\Delta\dot{X} = (m's/m_e + C_DS\rho\dot{z}/2m_e)\Delta\dot{X}_W \tag{29}$$

the equation of horizontal motion for balloons.[18] Since the response length of the balloon, or drag sensor, is $L = 2m_e/C_DS\rho$, the tuned lifting sensor resolution is $C_D/C_{L\alpha}$ times that of a drag sensor with identical fall velocity [determined by Eq. (3)]. For the sample configuration, $C_D/C_{L\alpha} = \frac{1}{37}$; thus, a tuned lifting sensor can fall about six times faster than a drag sensor and yet maintain the same resolution.

The tuning conditions, Eqs. (24) and (25), are functions of ρ and, with the assumptions of this analysis, cannot be met by a lifting sensor at every altitude; however, the tuned condition determines the maximum resolution, or bandwidth, of both tuned and untuned sensors, as shown in the next section.

Returning to the step response of untuned configurations, Fig. 5 shows the effect of decreasing ρ and increasing U. At 40,000 ft, the short-period frequencies are about the same, but the increased fall velocity has increased the wavelength, and the decreased density has decreased damping. The most serious consequence of the altitude change is that the short-period/path stability mode ratio has decreased. The wings improve wind response, but to a lesser extent than before. The 0.05-ft case does not overrespond to the input, for it is undertuned at 40,000 ft. Because of the higher U, the 10-fps wind represents a smaller α input and produces a smaller θ. At 60,000 ft, the step response has deteriorated further, and, by 100,000 ft, even the least stable configuration is too stable for the wings to be of value. A tuned sensor, which would have a response length of 400 ft, would require a SM of 0.002 ft, a number too small for serious consideration.

The step response gives a useful indication of wind sensitivity; however, in order to determine the resolution with which a wind profile will be measured, the methods of frequency response must be brought to bear.

Frequency Response

The wind response transfer function is used to determine the amplitude and phase characteristics of several cases as functions of sine wave frequency. Asymptotic corner frequencies are determined directly from the transfer function's zeroes and poles. Amplitude response curves are plotted as departures from the asymptotic approximations, whereas phase angles are plotted directly.

Typical frequency response curves are sketched in Fig. 6, with approximate locations of poles and zeroes noted. The

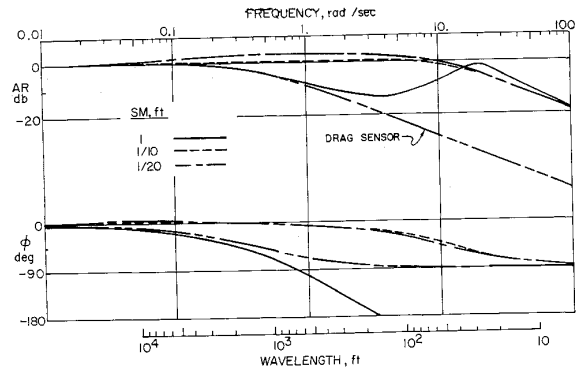

Fig. 7 Frequency response, amplitude ratio AR, and phase angle ϕ, of the lifting sensor at 5300 ft for three values of static margin. Curves for a drag sensor with identical fall velocity are shown.

most common case is shown in Fig. 6a. Beginning at low frequency, the amplitude asymptote breaks to -20 db/decade at the path stability pole, is restored to 0 db/decade by the first zero, rises to $+20$ db/decade at the second zero, and finally drops to -20 db/decade at the short-period pair. If $L_{\dot{\alpha}} \neq L_{\theta}$, the asymptote returns to 0 db/decade beyond the short-period frequency. In some instances, z_1 and z_2 combine to form a complex pair between their indicated locations. The actual amplitude curve is a continuous curve based on the asymptotes. The phase angle dips below 0°, reaching a relative minimum between the first pole and the first zero. It becomes positive beyond the second zero and then drops to $-90°$ past ω_{nSP}. Case a represents an underresponding sensor.

Case b overresponds to the wind. The prime difference between cases a and b is that λ_{PS} and z_1 are reversed. Consequently, the amplitude curve rises above 0 db. In some instances, ω_{nSP} and z_2 change places, but this does not change the shape of the curve markedly, for the singularities are close together. In every case computed, the first inversion corresponded to a reversal of the sign of the pitch numerator term B_1. It can be concluded that setting $B_1 = 0$ is the more important of the tuning conditions. Furthermore, B_2 is generally near zero, since $M_{\dot{\alpha}} \simeq M_{\dot{\theta}}$, and $L_{\dot{\alpha}} \simeq L_{\dot{\theta}}$. The phase angle response of case b is reversed at low frequency by the inversion of λ_{PS} and z_1 but is otherwise similar to case a.

The frequency response at 5300 ft is plotted in Fig. 7. For reference, the response of the drag sensor with identical fall velocity is also plotted. The drag sensor's amplitude response breaks to -20 db/decade at the path stability root; its phase angle drops to $-45°$ at the same point. The 1.0-ft sensor's amplitude curve begins in much the same way but rises to a peak near the short-period frequency. The dip in amplitude indicates that this model will sense the winds with wavelengths λ from 50 to 1000 ft poorly; thus, the wings do not work to advantage. The 0.1- and 0.05-ft sensors overrespond in the same interval, dropping to -3 db at a 40-ft wavelength. Note that all of the lifting sensors approach the same asymptote at high frequency. Since only M_{α} changes when SM changes, the ratio D_2/A_3, which determines high-frequency response, is constant. The location of the asymptote can be given by its intersection with the 0-db line. As there is an approximately tuned sensor in every set of cases, i.e., only $B_1 = 0$, Eq. (27) determines this intersection.

The effects of nonminimum phase zeros can be seen in the phase response of the 1.0-ft case. What little output occurs beyond the path stability root greatly lags the input and probably would be lost in practice. The 0.1- and 0.05-ft models have minimum phase zeroes, extending the onset of significant phase lag to the region of the short-period frequency. The criterion for insuring that only minimum phase zeroes occur (assuming $L_{\dot{\alpha}} = L_{\dot{\theta}}$) is that D_1 be of the same sign as D_0 and D_2.

The progressive deterioration with altitude noted in the step response reappears in Fig. 8. The high-frequency asymptote shifts to the left as the amplitude ratio drops and as the dip between the path stability and short-period frequencies becomes more pronounced. The responses of the 0.1- and 0.05-ft sensors are good at 40,000 ft, marginal at 60,000 ft, and not significantly better than the corresponding drag sensor at 100,000 ft. With respect to the time frequency scale, the wavelength shifts to the right as altitude and fall velocity increase. None of the sensors is good over the entire 100,000-ft interval.

Changes in the frequency response due to variations of individual parameters can be summarized. The effect of mass variation is the inverse of the air density's effect; thus, an increase in mass is comparable to an increase in altitude. Changes in L_{α} shift the 0-db corner frequency of the final asymptote, affecting the maximum resolution according to Eq. (27). Variations in M_{α} are inherently tied to the value

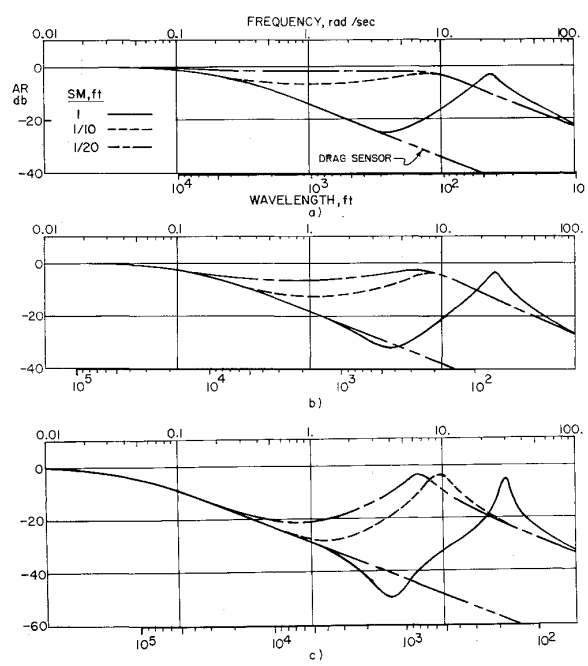

Fig. 8 Amplitude ratio response at a) 40,000 ft, b) 60,000 ft, and c) 100,000 ft.

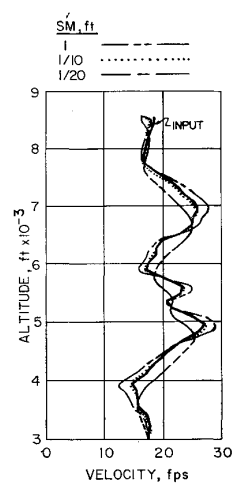

Fig. 9 Computed response of three lifting sensor configurations to the unsmoothed TD-64 wind profile.

of $M_{\dot{\theta}}$ by the aerodynamic tuning relation, Eq. (23). Changing U, which corresponds to changing $C_D S$, stretches or shrinks the frequency response curves, with negligible effect on the magnitudes of the amplitude and phase. Since the response length given by Eq. (28) is independent of U, the corner frequency remains fixed in the wavelength domain; however, the corner frequency shifts on the time scale. The path stability root varies as $1/U$ on the time frequency scale and as $1/U^2$ on the wavelength scale. Increasing I_y concentrates response energy in the short-period mode, but the high-frequency asymptote is only slightly altered. By comparison to the foregoing parameters, variations due to $M_{\dot{\alpha}}$, $L_{\dot{\alpha}}$, and $L_{\dot{\theta}}$ are negligibly small. The effects of $M_{\dot{\alpha}}$ are similar to those of $M_{\dot{\theta}}$. $L_{\dot{\alpha}}$ and $L_{\dot{\theta}}$ have minor effects on the maximum resolution and aerodynamic tuning.

Wind-Profile Response

The final test of the wind sensor is its ability to reproduce a wind profile. The three-degree-of-freedom digital computer program, which accepts an arbitrary wind-profile input and which solves the full equations of motion, computes wind velocity and shear response, as well as average ϵ and rms errors in the wind-profile estimate. For the error calculations, altitude rather than time was taken as the independent variable.

Using this program, the three sample configurations have been subjected to wind profiles. The TD-64 profile is representative of typical winds below 10,000 ft. The TN D-1821 profile[10] is an unusually severe one. A third profile representative of winds up to 100,000 ft is presented and discussed in the original paper (AIAA Preprint 65-15). Lifting sensor response to this profile showed less than 5% error over an altitude interval of 50,000 ft.

The first profile was originally measured by the radiosonde balloon that carried the experimental lifting sensor TD-64 to altitude. Since the target tracked was the sensor, suspended 40 ft beneath the balloon, it is likely that some of the detail of this profile is due to pendulum oscillations. Although the data probably are not valid for $\lambda < 1000$ ft, the detail is included for test purposes.

The computed results (Fig. 9) indicate the trends predicted by the frequency response of Fig. 7. The 1.0-ft model smears the peaks and lags the over-all profile by about 200 ft. The remaining models overrespond to the profile's oscillations but tend to smear the profile at the sharp changes produced by the straight-line approximation between data points. As these oscillations have primary wavelengths from 500 to 3000 ft, whereas the sharp changes introduce shorter wavelength components, this is the trend predicted by the frequency response. The rms errors between sensor horizontal velocity and the wind velocity for the 1.0-, 0.1-, and 0.05-ft cases are 2.06, 0.26, and 1.21 fps, respectively. The average errors are 1.71, 0.20, and 1.01 fps.

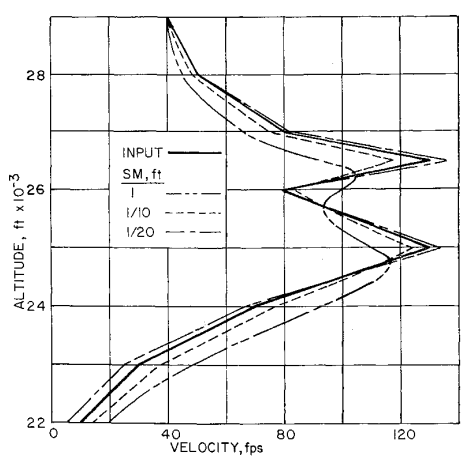

Fig. 10 Computed response of three lifting sensor configurations to the TN D-1821 wind profile.

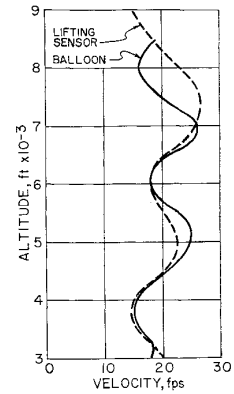

Fig. 11 Flight-test results for the TD-64 lifting sensor. Space-time displacement of the two profiles is less than 2 naut miles and 10 min. Measurement time of balloon 6 min; of lifting sensor 1 min. Balloon data have been smoothed to a minimum wavelength of 1000 ft.

The TN D-1821 profile was chosen because it presents a region of high shear with sharp peaks near jetstream altitude and because it affords a comparison with balloon responses in Ref. 10. This profile for the altitude layer from 20,000 to 29,000 ft is composed of constant shear ramps, with shear magnitudes of 0 to 0.1 fps/ft. The responses shown in Fig. 10 are consistent with the frequency response curves that bracket this layer. The 1.0-ft sensor has low amplitude response and significant lag in determining the peaks, but the low SM sensors exhibit lags <15 ft and amplitude responses close to the input velocity. The 0.05-ft sensor overestimates the peaks because it is overtuned in this layer. The rms errors, in the same order as before, are 13.9, 4.7, and 3.0 fps, and the average errors are 10.9, 3.8, and 2.4 fps.

The θ's and α's produced by this profile are probably as large as any that would be experienced in nature, and yet for the low SM sensors, $\Delta\theta \leq 6°$ and $\alpha \leq 0.76°$, with smaller values at points removed from the discontinuities between shear layers. For the 1.0-ft sensor, θ excursions up to 15° occurred.

The computed fall times for these configurations are in close agreement with an analytical expression based on Eq. (3). For any given profile, the variation between the three static margin cases is less than 1 sec. The lifting sensor required 63 sec to fall from 8500 to 3000 ft (TD-64 profile), 75 sec to fall from 29,000 to 20,000 ft (TN D-1821 profile), and 9 min 11 sec to fall from 100,000 ft to sea level.

Flight-Test Program

Four flight tests were made at the NASA Wallops Station. The sensors were assembled with rigid, erect frameworks, as shown in Fig. 1, and were carried to altitudes from 10,000 to 70,000 ft by standard radiosonde balloons. They were tracked by an FPS-16 radar. Two of the flights produced data consistent with the mathematical analysis presented here. In the other two, one sensor failed to separate from its radiosonde balloon, and the other apparently failed structurally shortly after release.

Since these sensors had high static margins, the wings did not work to full effect, and wind response is not significantly better than that of a drag sensor with the same fall velocity. However, the lower bound of lifting sensor response and the ability of the data collection system to determine horizontal velocity accurately enough to provide the wind profile are verified. The east-west component of the profiles indicated by the 1-ft sensor and its radiosonde balloon are shown in Fig. 11. Both profiles have been smoothed to a minimum wavelength of 1000 ft, which is consistent with the computer smoothing of the lifting sensor's radar data. The radiosonde

Table 1 Closure of iterative estimate of the TN D-1821 profile for three static margins

Static margin, ft	Error in successive estimates, fps											
	1st		2nd		3rd		4th		5th		6th	
	rms	ϵ	rms	ϵ	rms	ϵ	rms	ϵ	rms	ϵ	rms	ϵ
1.0	13.9	10.9	8.9	6.2	7.8	4.9	7.4	4.2	7.2	4.1	7.1	4.0
0.1	4.7	3.8	0.8	0.6	0.2	0.2	0.1	0.1	0.1	0.1	0.1	0.1
0.05	3.0	2.4	0.3	0.2	0.1	0.1	0.1	0.1	0.1	0.1	0.1	0.1

and lifting sensor profiles were measured 1 to 10 min apart, depending on altitude. Horizontal displacement between the measurements is less than 12,000 ft. Since there is no direct input-output relationship between the curves, because of the space-time displacement, the accuracy of the lifting sensor response cannot be determined. The agreement of the peaks between 3500 and 6000 ft indicates that the same trends were sensed by both sensors; however, the indicated amplitude ratios and phase differences are not precise.

Flight-test results for TD-65, a similar sensor with a static margin of 1.5 ft and a weight of 4.2 lb, are plotted in Fig. 12. Below 55,000 ft, the lifting sensor appears to have sensed all the fluctuations with $\lambda > 1000$ ft which were sensed by the radiosonde balloon; above this altitude, TD-65 loses detail. The over-all lag tendency of the high SM sensor predicted earlier is evident.

Data Correction Technique

With a knowledge of a sensor's physical characteristics and of the dynamical process of measuring the wind, the estimate of a wind profile can be improved using an iterative technique based on a trajectory program, such as the one used in the previous section. The measured horizontal velocity profile of the wind sensor is used as a first estimate of the wind profile, and the wind response of the lifting sensor's mathematical model is computed. This response is compared to the actual response, and the difference is added to the old profile to provide an updated estimate. The TN D-1821 profile was used as a test input for the three sensor configurations. Table 1 shows that two iterations accomplish the major reduction in error. The plotted results, included in AIAA Preprint 65-15, indicate that iteration slowly minimizes the lag of the 1.0-ft sensor. By the second iteration, the wind estimate overshoots the peaks, as a result of improper convergence of the iteration. Although the rms and average errors decrease, the overshoot continues to get worse, at least through the fourth iteration. The wind estimates from the 0.1- and 0.05-ft sensors are substantially better, to the extent that it is difficult to distinguish even the first iteration from the wind input. In the few cases considered, this technique appears to reduce errors by at least an order of magnitude, except in areas of improper convergence, which require further study.

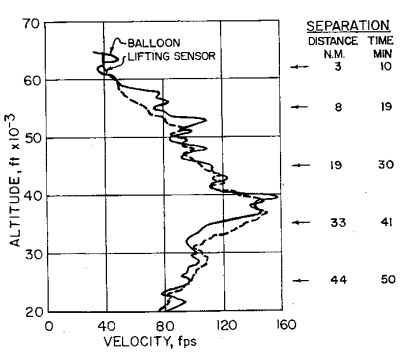

Fig. 12 Flight-test results for the TD-65 lifting sensor. Measurement time of balloon: 46 min; of lifting sensor: 3 min.

Conclusions

The lifting sensor is capable of measuring the wind profile below 100,000 ft in 10 to 15 min. Unlike the drag sensor maximum wind-profile resolution is determined by C_{L_α} rather than by C_D. Consequently, the lifting sensor's wind response is more than an order of magnitude better than that of a drag sensor with equal fall velocity. Amplitude and phase fidelity for input wavelengths between the path stability mode and maximum resolution is primarily determined by the pitch moment stability derivatives and is a function of altitude. Numerical calculations indicate that a lifting sensor can measure a typical wind profile with an rms error of less than 5% over a 50,000-ft altitude interval (neglecting data collection system errors, which are of the same order). The mean wind profile can be measured up to 100,000 ft, but detail is lost because of diminishing pitch damping.

It is possible to improve the wind profile further and to extend the useful altitude interval by correcting sensor dynamic errors with an iterative technique. Except in areas of improper convergence, apparently caused by excessive lag in the sensor output, the iteration reduces errors by at least an order of magnitude.

A limited flight-test program verified the lower bound of lifting sensor response and the ability of the data collection system to determine the sensor's horizontal velocity accurately enough to provide the wind profile. In future flight tests, low SM sensors should be used, with higher resolution in the computer smoothing of radar data. It will be necessary to reduce the space-time displacement between the sensor profile and the reference wind profile in order to obtain quantitative amplitude and phase response data. Wind response could be improved by augmenting pitch stability, e.g., by canting the sensor's wings to induce spinning and, thus, a measure of gyroscopic stability. Active systems employing rate gyros and control surfaces or varying static margin can be envisioned but may be too complex for consideration.

It is concluded that, by virtue of the short measurement time, a near-vertical measurement over the launch site, high resolution, and all-weather utility, the lifting sensor provides a superior means of measuring wind profiles for rocket prelaunch operations.

References

[1] Reisig, G. H. R., "The significance of atmospheric ballistics in rocket technology," NASA TN D-1830 (1963).

[2] Henning, A. B., Lundstrom, R. R., and Keating, J. C., "A wind-compensation method and results of its application to flight tests of twelve Trailblazer rocket vehicles," NASA TN D-2053 (1964).

[3] James, R. L. Jr., and Harris, R. J., "Calculation of wind compensation for launching of unguided rockets," NASA TN D-645 (1961).

[4] Henry, R. M., Brandon, G. W., Tolefson, H. B., Lanford, W. E., "The smoke-trail method for obtaining detailed measurements of the vertical wind profile for application to missile-dynamic-response problems," NASA TN D-976 (1961).

[5] Scoggins, J. R. and Vaughan, W. W., "Problems of atmospheric wind inputs for missile and space vehicle design," J. Spacecraft Rockets **1**, 181–184 (1964).

[6] Connor, F., "Study of high resolution wind measuring systems—Phase I survey," NASA Contractor Rept. CR-61035 (December 1964).

[7] Hibben, R. D., "Wind shear measurement techniques," Aviation Week Space Technol. **80**, 43 (1964).

[8] Larrabee, E. E., "Interpretation of wind shear probe data," Measurement of Wind Shear, Final Report Signal Corps Contract DA-36-039 SC-75064 (1959).

[9] Henry, R. M. and Scoggins, J. R., "Self-induced balloon motions," Astronaut. Aerospace Eng. **1**, 5 (1963).

[10] Reed, W. H., III, "Dynamic response of rising and falling balloon wind sensors with application to estimates of wind loads on launch vehicles," NASA TN D-1821 (1963).

[11] Scoggins, J. R., "High resolution wind measurement: a launch design problem," Astronaut. Aerospace Eng. **1**, 106–107 (1963).

[12] Scoggins, J. R., "An evaluation of detail wind data as measured by the FPS-16 radar/spherical balloon technique," NASA TN D-1572 (1963).

[13] Etkin, B., *Dynamics of Flight* (John Wiley and Sons, Inc., New York, 1959), pp. 393–400, 94–126, 321–322.

[14] Nielsen, J. N., *Missile Aerodynamics* (McGraw-Hill Book Co., Inc., New York, 1960), Chap. 10.

[15] Donovan, A. F., Lawrence, H. R., Goddard, F. E., and Gilruth, R. R., "High speed problems of aircraft and experimental methods," *High Speed Aerodynamics and Jet Propulsion* (Princeton University Press, Princeton, N. J., 1962), Vol. VIII, pp. 108–112.

[16] Seckel, E., *Stability and Control of Airplanes and Helicopters* (Academic Press Inc., New York, 1964), pp. 49–50, 163–164.

[17] Jex, H. R. and Tennant, J. A., "Dynamic response of nonspherical windsondes," Systems Technology Rept. TR-245-1, NASA Contract NAS-5294 (1964).

[18] Eckstrom, C. V., "Theoretical and engineering development of Jimsphere wind sensor," NASA Contract NAS8-11158 (January 1964).